Highly interpretable machine learning framework for prediction of mechanical properties of nickel based superalloys

Nikhil Khatavkar and Abhishek Kumar Singh[*]
Materials Research Centre, Indian Institute of Science, Bangalore 560012, India

Superalloys are a special class of heavy-duty materials with excellent strength retention and chemical stability at very high temperatures. Nickel-based superalloys are used commercially in aircraft turbines, power plants, and space launch vehicles. The optimization of mechanical properties of alloys has been traditionally carried out using experimental approaches, which demand massive costs in terms of time and infrastructure for testing. In this paper, we propose a method for mechanical property prediction of Ni-based superalloys by learning from past experimental results using machine learning (ML). Five highly accurate ML models are developed to predict yield strength (YS), ultimate tensile strength (UTS), creep rupture life, fatigue life with stress, and strain values. We have developed an extensive database containing mechanical properties of over 1500 Ni-based superalloys. Basic material parameters such as the composition of the alloy, annealing conditions, and testing conditions are also collected and used as features for developing the ML models. The prediction root mean squared errors for the YS, UTS, creep, and fatigue life models are 0.11, 0.06, 0.19, 0.22, which are minimal, leading to a highly accurate estimation of the target values. These ML models are highly transferable and require a minimum number of input features. In addition, feature analysis performed by SHapley Additive exPlanations (SHAP) for individual properties reveals the relative significance of each descriptor in deciding the target property. We demonstrate that a unified and highly accurate ML framework can be developed using common features for all mechanical properties. The models are developed on experimental data, making them directly applicable for industries.

I. INTRODUCTION

Nickel-based superalloys have emerged as the most favored class of materials for applications involving high strength along with superior creep and fatigue properties at high temperatures. Ni-based superalloys enable systems to operate at very high temperatures, which leads to high efficiency and lower fuel consumption [1]. Some of the modern superalloys can operate at temperatures over 80% of the melting temperature, extending their operating temperatures over 1200 °C [2–4]. As a result, superalloys are heavily employed in gas turbines for aircraft propulsion engines and electricity generators [5–7]. These superior properties are due to several decades of optimization of composition and microstructure s [8,9]. Initially, the enhancement of properties resulted from improved microstructures by employing sophisticated casting techniques. The directionally cast superalloys were a noticeable improvement over the wrought alloys as the grain boundaries in the direction of load can be effectively eliminated to reduce the risk of nucleation of cracks. The microstructural design was improved further by producing single-crystal superalloys. In addition, vast enhancement in strength and creep/fatigue resistance is made possible by optimization of the precipitate γ' phase [10,11]. The presence of a γ' phase in addition to the matrix γ phase in this

generation of superalloys imparts the required strengthening through precipitation hardening and blocking dislocation motion [12,13]. Optimization of composition of the superalloy can also provide better mechanical properties by solid solution strengthening and influencing the volume fraction and distribution of γ' precipitates. Several elements such as Mo, W, Ta, Ti, and Nb are beneficial for the precipitation process, and the lattice mismatch induced between the γ and γ' due to the addition of these elements leads to dislocation immobilization at the boundaries [14,15]. However, this crucial optimization process of microstructural and compositional parameters is painstakingly slow due to the vast compositional space. In addition, experimental determination of creep rupture lifetime and fatigue cycles to failure is also highly time and cost intensive.

The introduction of machine learning (ML) in the field of material science in the last few years has led to significant acceleration in the process of materials discovery [16–19]. ML utilizes several algorithms to learn the dominant patterns in the existing data and connect them to the desirable property. These patterns are then used to predict the property of a new set of data. ML has been used successfully in the past to predict diverse material properties such as band gaps [20–22], band edges [23], lattice thermal conductivity [24], glass transition temperatures [25], dielectric constants [26], and Vickers hardness [27,28]. Recently, ML has also been successfully applied to high entropy alloys for prediction of phase, hardness, and solid solution forming ability [29–31]. Moreover,

*abhishek@iisc.ac.in

ML methods have successfully optimized several properties of nickel-based superalloys such as phase fraction of γ' phase, density, solvus temperature of the γ' phase, and lattice mismatch of the γ and γ' phases [32–34]. These properties of superalloys play an important role in designing turbines with enhanced lifetimes. ML was also used to predict the chemical composition of the different phases of nickel-based superalloys [33]. In addition, the most important criteria for consideration of any material for turbine applications are the simultaneous presence of high yield strength (YS), fatigue, and creep life at high temperatures. Approaches which can simultaneously predict and optimize the properties of interest for Ni-based superalloys exist [32]. However, it will be highly beneficial if analysis of features is performed rigorously for thorough understanding of the ML models developed.

In this paper, we develop a unifying ML modeling scheme to predict the mechanical properties of nickel-based superalloys. The mechanical properties include YS (MPa), ultimate tensile strength (UTS) (MPa), creep rupture life (hours), and fatigue life (number of cycles). These four properties are essential and are widely studied while selecting components for heavy-duty applications. It is desirable to have the largest possible values for these properties while in operation; however, it is usually observed that these properties have conflicting requirements in terms of compositions and treatment. For instance, increasing the creep rupture life of a material may lead to fracture vulnerability due to fatigue. In the ML models developed, these properties can be calculated simultaneously using compositions, treatment conditions, and testing conditions. The ML models use minimal data as input, making it easy to use and highly transferable across different properties. ML models are developed using Gaussian process regression (GPR) for YS, UTS, and creep rupture life. Moreover, the testing conditions for determining fatigue life include stress and strain amplitude [35–37]. Therefore, separate ML models are developed for including stress and strain as independent features. Finally, using feature engineering, we perform in-depth feature analysis and identify a set of features which are highly correlated to all the mechanical properties considered in this paper. This set of features is employed to develop a unified ML model framework that simultaneously predicts all the mechanical properties.

II. METHODOLOGY

A database was initially built for Ni-based superalloys. The data utilized for developing the ML model development is taken from literature [13,35–103]. This database contains the compositions, annealing schedules, and testing conditions as the features/descriptors for developing the ML models and the mechanical properties as the final target property. The features selected are easily available in any experimental study. The data set contains 349 values for YS, 248 for UTS, and 383 for creep rupture life along with their corresponding features. Moreover, 318 values exist for fatigue life with stress and 384 for fatigue life with strain. All the data collected contain 1610 values from recent literature, and all data was selected only if all the mentioned descriptors and at least one of the target properties of a material were present. The sources (DOIs) of the data are also presented in Supplemental Material

Table 1 [104]. The compositions of the superalloys consist of 24 elements recorded in weight percentages. It is ensured that the sum of all the elements must add up to 100%; otherwise, the data is not considered further. The annealing schedule considers the two-step procedure, which is generally followed for Ni-based superalloys. The annealing temperatures are recorded in Celsius and denoted as T_{an}^1 and T_{an}^2, respectively. Similarly, the annealing times are recorded in hours and denoted as t_{an}^1 and t_{an}^2, respectively. Solutionizing treatment is also a widely reported parameter for Ni-based superalloys, in which the alloy is heated above its solvus temperature. However, this treatment is only a precursor step in the precipitation hardening process before annealing. The material properties change drastically after the annealing process is complete. Therefore, we choose not to include solutionizing treatment for this paper. The distribution of the compositions and the annealing schedule is presented in Supplemental Material Table 2. In addition to the composition and heat treatment parameters, we also include composition-averaged elemental features as descriptors in this paper. The elemental features in this paper are easily available and provide additional sets of information that can be highly relevant for this study. Thus, the database consists of 43 features which are presented in Supplemental Material Table 3. The target properties are converted to log values before further process. To keep user input to a bare minimum, selecting only the most basic features for this paper becomes crucial. Therefore, any other input derived from other experiments or modeling is included in the development of ML models.

Traditional experimental methods of mechanical property determination are specialized and accurate; however, these methods are highly time intensive and costly when applied for exploratory research. The creep-fracture life of some materials can reach 10^4 to 10^5 hours, and fatigue life can reach over 10^8 cycles. The sheer amount of time required alone makes the swift determination of mechanical properties a challenging task. To circumvent this, we use the database to build ML models for faster prediction of the properties as compared to experiments. One of the crucial aspects of ML is to identify the features which are highly relevant for the prediction of the target properties. In this paper, the least absolute shrinkage and selection operator (LASSO) is employed for feature selection [105]. LASSO is a regression and regularization technique that determines the weights of features by minimizing the ordinary least squares (OLS) term subject to the L1 penalty term, which can be represented as

$$\min\left\{\frac{1}{N}||\mathbf{y} - \mathbf{wx}||^2 + \lambda||\mathbf{w}||_1\right\}, \quad (1)$$

where x, y, N, λ are the feature vector, target, the size of data set and penalty parameter, which controls the shrinkage of the coefficients, respectively. Larger values of λ lead to larger reduction in the number of features. The optimization of the parameter λ is performed manually. LASSO is an embedded feature selection method that removes features that are either redundant or are poorly correlated to the property [106]. Several unique methods are also available for feature selection such as the data-driven multilayer feature selection method (DML − FS$_{dek}$) [107]. Since the number of features in this

work is manageable, we proceed with LASSO for the feature selection process.

For the prediction of the properties, we have employed GPR based on the Bayesian inference approach. In GPR, the algorithm chooses the suitable functional form, which makes it a nonparametric approach [108]. Instead of determining fixed parameters for a function, GPR employs output distribution from various functions using a Gaussian process distribution. The possibility of selecting the functions poses a problem since the space of possible functions is infinite. Therefore, some initial assumptions are made to restrict the search in functional space, known as prior. This space is defined such that the mean of all functions is zero, while the standard deviation throughout the space is $\sum_p$ and can be represented as

$$w \sim \mathcal{N}(0, \Sigma_p). \qquad (2)$$

The target output in GPR takes the following form [109]:

$$y = \hat{y} + \epsilon, \qquad (3)$$

where $\hat{y}$ represents the Gaussian distribution for target prediction, which is to be determined, and ϵ is a Gaussian distribution of noise with zero mean and a constant variance. The joint Gaussian distribution for the target property can be represented as

$$\hat{y}(x) = N(\mu(x), k(x, x')), \qquad (4)$$

where $\mathcal{N}$ represents a normal multivariate distribution with $\mu(x)$ mean and $k(x, x')$ covariance. The noise assumption with the model gives rise to likelihood. Likelihood is defined as the probability density of parameters fitting the given data and is represented as

$$p(y|X, w) = \mathcal{N}(X^T w, \sigma_n^2 I) \qquad (5)$$

where X is the feature vector ($X = (x_1, x_2, ..., x_n)^T$). The weights (w) are updated to increase the probability of the function fitting the data and are represented by the posterior as

$$p(w|y, X) = \frac{\text{likelihood} * \text{prior}}{\text{marginal likelihood}}, \qquad (6)$$

where the marginal likelihood is a constant value independent of the weights. Posterior captures all the information from likelihood and prior. If only numerator terms are considered, the posterior assumes the form of

$$p(w|y, X) \sim \mathcal{N}\left(\bar{w} = \frac{1}{\sigma_n^2} A^{-1} Xy, A^{-1}\right), \qquad (7)$$

where $A = \sigma_n^{-2} XX^T + \Sigma_p^{-1}$. This is a Gaussian distribution with $\bar{w}$ as the mean and A^{-1} as the covariance matrix. This method scales poorly as $O(n^3)$ due to the computationally costly step of multiplication of XX^T and inversion of the matrix A. Instead of the multiplication, a kernel trick is applied to reduce the number of calculations involved. For implementation, several kernels such as the polynomial (quadratic), radial basis function (RBF), dot-product, and Matern kernels are available. The kernel selection is essential for the accuracy of the final ML model. In this paper, we have evaluated all the kernels for ML model development suitable for the data set.

Finally, the predictions are made for unknown data by performing an average over all the functional values, weighted by posterior probability density. The final distribution has the form of Gaussian function, which is represented as

$$p(f_*|x_*, X, y) = \mathcal{N}\left(\frac{1}{\sigma_n^2} x_*^T A^{-1} Xy, x_*^T A^{-1} x_*\right), \qquad (8)$$

where x_* is the input for the prediction of the target property through the function f_*.

It is important to analyze the built ML models for obtaining the dominant trends that help to maximize the target properties. After training efficient ML models, analysis of the ML models is done using the Pearson correlation coefficients (PCCs). The PCC is defined as [110]

$$\rho(X, y) = \text{cov}(X, y)/\sigma_X * \sigma_y \qquad (9)$$

where cov() is the covariance function and σ is the variance. X and y denote the feature and target properties under consideration, respectively. The PCC measures the linear correlation between the target property and individual features. The value of the PCC ranges between -1 to 1 for normally distributed standardized data. Positive correlation implies that as the value of feature X increases, the value of y will also increase. A larger magnitude indicates a stronger correlation between the feature and target properties. The GPR-based ML algorithms and PCCs are implemented on Python using the SCIKIT-LEARN ML library [111].

III. RESULTS

A. Data preprocessing

The data collected was subjected to filtering conditions to ensure that only high-quality and valid data is used for the ML modeling. The validity of compositions was ensured by summing all elemental compositions. The data set was selected if the elemental compositions add up to 100%. Only weight percentages are used for composition in this study as it is the most common form of representation in literature. Some inaccuracies pertaining to individual element concentrations were also corrected by referring to the alternative sources as presented in Supplemental Material Table 4. Next, standardization of the features was performed using the standard scalar feature in the Python SKLEARN library [111]. Standardization is done to bring all features to a uniform scale such that the mean of the feature distribution is zero and the standard deviation is one. The range of values after standardization is presented for all features for different properties in Supplemental Material Fig. 1.

B. ML model development

The purpose of our paper is to develop a unified and robust approach for the prediction of mechanical properties that are most crucial while evaluating the usefulness of a superalloy in demanding applications. The schematic of the work is depicted in Fig. 1, showing the important steps in this approach. The collected data is segregated according to the target property and ML models are developed using the algorithms discussed in the Methodology section.
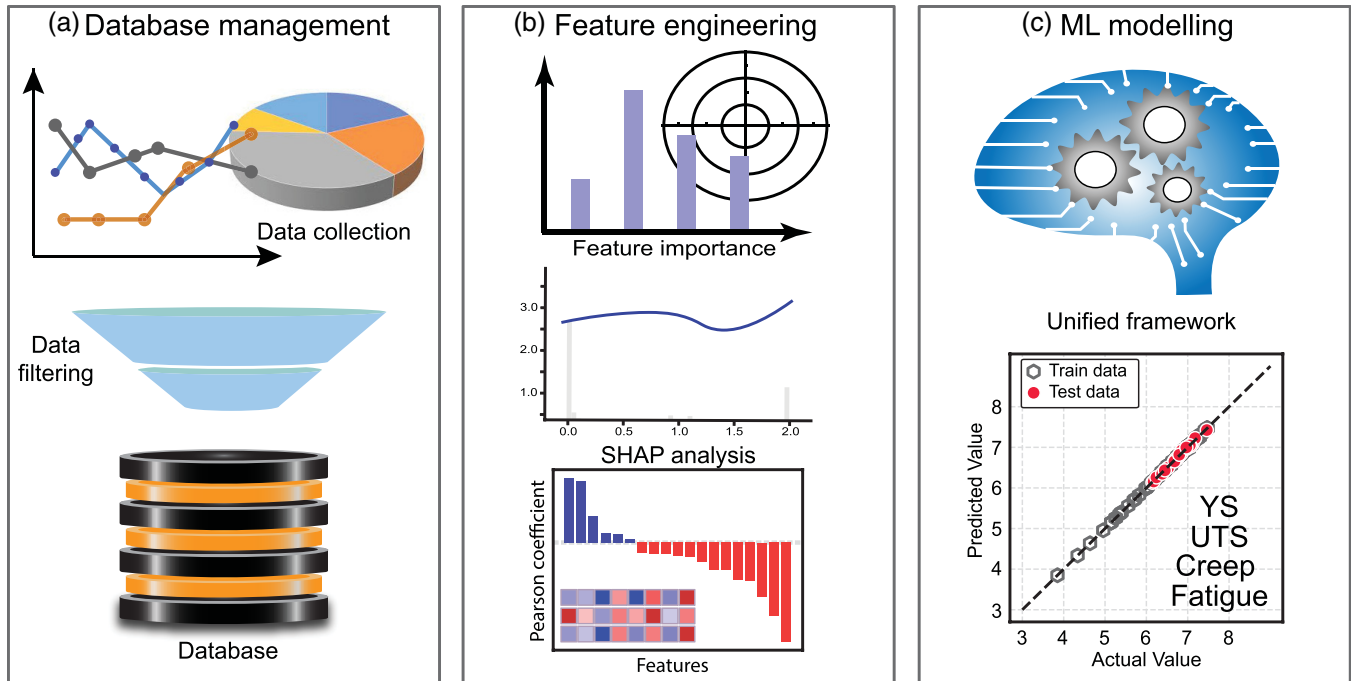
FIG. 1. Schematic representation of the work. (a) A database is established with experimental data from the literature. The data is subjected to rigorous filtering conditions and standardization. (b) Feature engineering is performed for individual data sets to identify the relevant descriptors and study the effect on the target property. (c) ML models are developed for individual properties using the identified crucial features.

To determine the ML models' accuracy, we use the coefficients of determination (R^2), and root mean squared error (rmse). The coefficient of determination is defined as the proportion of variation of the dependent variable (target property), which is captured by the variations in independent variables or features. R^2 is an important parameter, which gives us the quantitative value of the quality of the ML models developed. R^2 is defined as

$$R^2 = 1 - \frac{\sum_i (y_i - y_i')^2}{\sum_i (y_i - y_{mean})^2}, \qquad (10)$$

where vy_{mean} is the mean of all outcomes. R^2 ranges between 0 to 1, where 1 represents best fitting of model while 0 represents minimum fitting. The rmse for a given data set is defined as the standard deviation of the residual errors between predicted and actual values. It can be represented as

$$\text{rmse} = \sqrt{\frac{1}{n} \sum_i^n (y_i - y_i')^2}, \qquad (11)$$

where n is the number of individual data, y_i is the actual value, and y'_i is the predicted value. rmse is preferred over the other absolute errors as it assigns greater priority to the largest errors due to the squared term. The minimum value of rmse represents that the ML model has a high prediction accuracy.

Initially, the ML model is developed using GPR for the YS of superalloys. The data was split in a training and testing set in the ratio of 90:10, and important features were selected using LASSO. To select the most important features for training the ML models, the λ parameter in LASSO was varied from 0.01 to 0.3. The best results for the λ value for all the properties along with the LASSO score is presented in Supplemental Material Table 5. It is found that increasing the λ to a larger value excludes the important features. Hence, the λ value is set to 0.01 for building ML models for YS.

The result of the ML model for different kernels is presented in Table I. It can be observed that the GPR model that employs the quadratic kernel performs better than the other kernels. The GPR model with a quadratic kernel delivers highly accurate predictions for YS on the training and test data with R^2 of 0.97/0.95 (train/test data) and rmse of 0.11/0.11. Moreover, the GPR model with the Matern kernel also performs well with R^2 of 0.96/0.92 and rmse of 0.12/0.13. In comparison, GPR models with RBF and dot-product kernels perform poorly. The rmse for dot product and RBF kernels are 0.38 and 0.18, which are significantly larger than the quadratic and Matern kernels. The results are analogous to other works, where the estimation of the thermal conductivity of frost is performed using GPR and Matern and quadratic kernels, producing highly accurate predictions [112]. Figure 2(a) depicts the performance of the GPR model, where it is observed that most of the testing data lie near the 45° dashed line.

The ML model developed in this paper employs 17 LASSO-selected features. This feature set includes 14 compositional features, two annealing parameters, and the temperature at which YS is measured. Individual PCCs of selected features are shown in Fig. 3. The compositions of Nb, Fe, Cr, Mo, and Zr are directly correlated with the YS, implying an enhancing effect through the addition of these elements. These elements are useful in providing strength to superalloys through solid-solution strengthening. These elements strengthen the γ matrix by impeding the movement of the

TABLE I. Performance of GPR models with different kernels for the mechanical properties (Bold fonts represent the best values for the mechanical properties).

Property	Matern		Dot		Quadratic		RBF	
	R^2	rmse	R^2	rmse	R^2	rmse	R^2	rmse
YS	0.96/0.92	0.12/0.13	0.59/0.71	0.38/0.38	**0.97/0.95**	**0.11/0.12**	0.98/0.92	0.18/0.19
UTS	0.98/0.98	0.07/0.08	0.58/0.60	0.33/0.33	**0.99/0.98**	**0.04/0.06**	0.89/0.89	0.17/0.17
Creep	**0.95/0.92**	**0.17/0.19**	0.52/0.48	1.24/1.26	0.99/0.77	0.04/0.67	0.98/0.96	0.22/0.37
Fatigue stress	**0.96/0.96**	**0.32/0.32**	0.84/0.78	1.51/1.51	0.99/0.88	0.11/1.10	0.98/0.90	1.01/1.04
Fatigue strain	**0.95/0.92**	**0.22/0.22**	0.52/0.56	1.54/1.56	0.96/0.96	0.44/0.40	0.92/0.92	0.63/0.61

dislocation. The effect of the strengthening depends on the difference in the atomic radius. Most of the selected elements have diameters larger than Ni, leading to high strengthening. Co and Ti are slightly negatively correlated, indicating that adding these elements does not lead to significant changes in the YS. The positive correlation of annealing time and temperatures with YS in Fig. 3 points to the relative dynamics of formation and distribution of the γ' phase. An increase of annealing temperature leads to higher nucleation and growth of the γ' phase in the material, leading to enhanced YS through precipitation hardening [113]. However, an increase of annealing time beyond a specific limit leads to coalescence

of the γ' phases leading to large precipitate diameters, which is detrimental to the superalloy. Therefore, a proper balance in the annealing time and temperature is necessary to maintain high YS. In most metals, the YS decreases with increasing temperature. The decrease is attributed to activation of dislocation motion that assists plastic deformation at high temperature [114]. However, superalloys exhibit a peculiar phenomena known as the yield point anomaly, where the YS of the material increases with temperature up to a specific limit [115,116]. The data used in this paper contain several observations from this temperature range, and therefore the larger values of YS obtained at the higher temperatures make
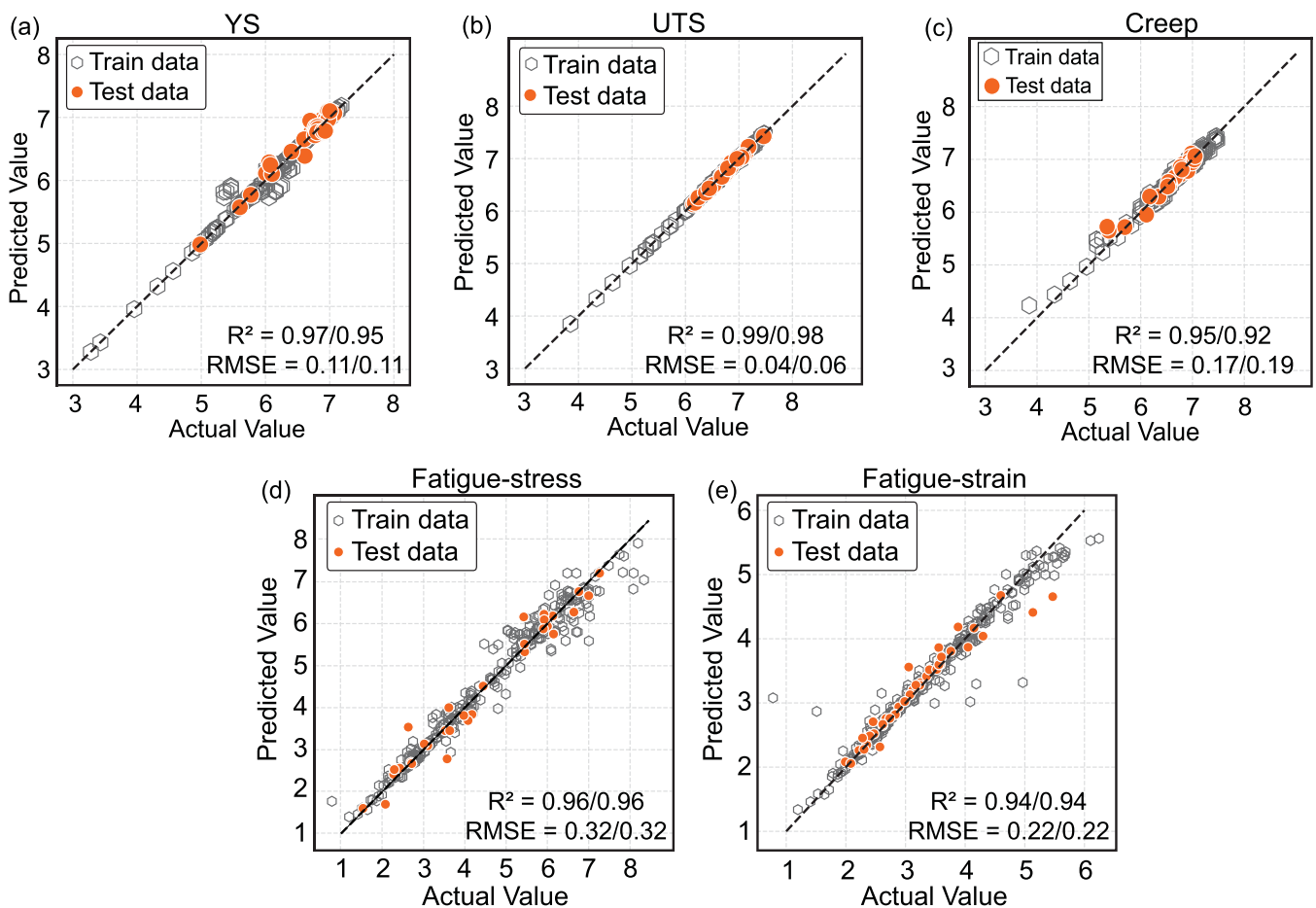

FIG. 2. The actual versus predicted values of best GPR models for (a) YS, (b) UTS, (c) creep, (d) fatigue with stress as feature (fatigue stress), (e) fatigue with strain as feature (fatigue strain). The data in all the mechanical properties lies near the black line, which implies that the ML models are highly accurate.
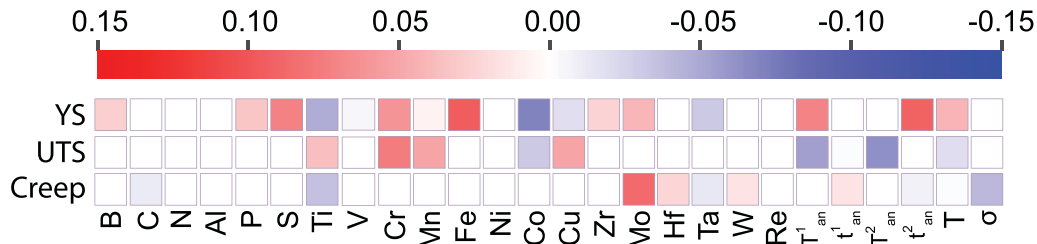
FIG. 3. Feature importance of composition and experimental conditions (stress and temperature of experiment) for the prediction of YS, UTS, creep rupture life. The correlations are presented as heat map for individual features.

the correlation of YS with temperature positive. Our ML model predicts the yield point anomaly of Ni-based super-alloys with reasonable accuracy as shown in Supplemental Material Fig. 2.

In literature, the estimation of YS analytically is done by constructing mathematical models using fixed composition or the majority elements in the superalloy such as Ni, Co, and microstructural features such as the γ and γ' phase distributions, volume fractions, and temperature [117–119]. These models are specialized for a particular set of compositions or specific precipitate shapes, making them highly accurate provided the assumptions of composition and precipitate geometry hold [120]. However, the validity of these models remains untested for different experimental conditions. We have approached this problem with a general and much less time-intensive procedure by applying data-driven ML models.

Previously, ML model development for determining the YS of superalloys was carried out using small subsets of data, leading to a higher bias toward specific compositions [121]. Moreover, the recent availability of several highly specialized ML algorithms generates a need to explore further improvement possibilities. To develop this model, we included the data from all the generations of superalloys to reduce the inherent bias the ML algorithm may acquire for certain compositions. The resulting prediction error of YS of 0.11 on a logarithmic scale, which translates to 1.2 MPa, is the lowest achieved among all the ML or analytical models developed.

The next property under consideration is the UTS. The data set for UTS, which consists of 41 features, is reduced initially using LASSO. The optimum result was obtained at λ value of 0.05, which reduced the number of features to eight. Using these features, ML models were developed using GPR employing different kernels. The best results for the ML models developed using different kernels are shown in Table I. The models developed using quadratic, Matern, and the RBF kernels show low rmse values. However, the R^2 value of the RBF kernel is considerably low (0.89/0.89) compared to the Matern and quadratic kernels. The ML model obtained the best results with the quadratic kernel having R^2 of 0.99/0.98 and rmse of 0.04/0.06. These results for the prediction of UTS are unprecedented, with minimal errors of prediction in log scale. When converted to a normal scale, the values show an error of 1.09/1.14 MPa, which indicates a considerable improvement in accuracy when the entire range of the property is considered. The true versus predicted values for the best ML model for UTS are shown in Fig. 2(b). The plot confirms that

the ML model captures the trend in the data set with a high degree of accuracy.

To study the effect of the selected features on the UTS, we examine their Pearson's correlation coefficient as shown in Fig. 3. Elements that provide solid solution strengthening lead to an increase in the UTS. Therefore, Ti, Cr, and Mn show a positive correlation with the UTS. The presence of trace amounts of carbon also leads to an increase of UTS due to the formation of hard carbide phases. The carbide phases hinder the dislocation movements and inhibit the sliding of grains relative to each other, thereby increasing the strength of superalloys [122]. At the same time, the effect of excessive annealing is detrimental for the UTS. An increase of annealing time/temperature leads to the formation of secondary γ' phases, which are generally larger in dimensions than the primary γ' phase. This increase in size is responsible for the deleterious effect on the UTS at room temperatures [123]. The negative correlation of measurement temperature with the UTS is a complex phenomenon [124] and can be attributed to the shearing of the γ' phase after the YS is reached. This effect is enhanced for higher temperatures and larger precipitate phases.

To serve as a component of the turbine, a material must bear heavy loading at high temperatures, which can be estimated by creep strength [125,126]. Creep strength is one of the most important and widely studied superalloy properties. Consequently, several models for predicting the creep of superalloys exist that employ a wide variety of input properties of the material [127–130]. The primary role of creep resistance is attributed to the more prominent presence of the γ' phase, which provides resistance to the defect diffusion [131]. Larger precipitate sizes and small γ channels are beneficial for increasing the creep resistance of superalloys [131]. Several analytical models sensitive to the compositional and microstructural properties have been proposed for the simulation of creep in two-phase superalloys [132–135]. Although accurate and sensitive to specific compositions, these models fail to capture the broader attributes that lead to significantly larger rupture lives. To circumvent the problem, data-driven models are being employed to predict creep rupture life of various high-temperature alloys [136–138]. This has enhanced the capability of making an informed prediction of the rupture life of superalloys. Liu *et al.* accurately predicted the creep rupture life of Ni-based single crystal alloys using the divide and conquer self-adaptive (DCSA) ML approach, where initially the data was clustered according to the creep mechanisms and further optimal ML models were developed for

prediction of the creep life. Similarly, creep life has also been predicted using neural networks combined with Monte Carlo techniques [138]. Our aim is to explore approaches that can provide highly accurate results while simultaneously reducing the complexity of the model. Therefore, in this paper, we develop ML models for creep rupture life using the most basic features used in experiments and study the dependence of rupture life on its composition, annealing parameters, and measurement conditions. Using LASSO, the most effective features are selected, then utilized to build ML models.

It is observed that for the prediction of rupture life of superalloys, the GPR model with the quadratic kernel yields the lowest rmse value for the training data set. However, there is a significant difference between the train rmse (0.04) and test rmse (0.67). The difference between the R^2 values of the train data (0.99) and test data (0.77) is also significant. This difference between the test/train rmse and R^2 values in the GPR model with the quadratic kernel indicates overfitting. Overfitting occurs when the ML algorithm fits the noise and the training data, leading to the failure in the accurate prediction of test data. The GPR model with Matern kernel is the most accurate model with R^2 of 0.95/0.92 and rmse of 0.17/0.19. Figure 2(c) shows the true versus predicted values for the GPR model. The data lies along the line confirming the model's accuracy.

From Fig. 3, it is clear that the elements responsible for the formation of the γ' phase show a positive correlation with the rupture life. This is expected as precipitate phases such as the γ' and carbide phases reduce creep rates. The presence of precipitate phases impedes both dislocations' movement and diffusing atoms while resisting the grain reorientation. Therefore, the addition of these substances is expected to increase creep strength. A critical aspect of the models is that the compositions of Re and Ru are not identified as important features. This trend is surprising since the successive generations of Ni-based superalloys are based on the addition and optimization of these elements from the 1980s [8]. On closer analysis of the collected data, it is observed that the composition of both these elements is either usually fixed near three wt % in experiments or the older generation of the superalloys; these elements are absent. This leads to the exclusion of both these elements from the ML models as the minimal variance is encountered with the target property. However, adding these elements in small quantities is beneficial for creep strength. The effect of Re and other elements is discussed in detail in the next section. In experiments, carbon is usually present in trace quantities to enhance creep properties [139,140]. However, the larger composition of carbon has been deemed as detrimental for creep properties due to the excessive formation of brittle MC, $M_{23}C_6$ and M_4C_3 phases at grain boundaries. Therefore, the negative trend presented by our ML model is in agreement with the experimental observations on rupture life [140]. In addition, the negative correlation of both creep stress and temperature of creep is an obvious conclusion analogous to empirical models.

The next model was developed to predict fatigue life of superalloys. Fatigue is also one of the most critical and widely studied properties. The engine components experience variations of loading conditions during the various stages of operation, making the study of fatigue at elevated temper-

atures in addition to the creep necessary. In the literature, we found that the reported fatigue parameters include the temperature of measurement, stress range, stress amplitude, and strain range. The presence of two different parameters based on stress and strain makes it challenging to fit a single ML model since the direct conversion of stress range to strain range and vice versa is not possible. Owing to a large amount of data in both cases, we build two separate ML models for the two regimes. The first ML model uses stress range, temperature, annealing conditions, composition, and elemental features as the descriptors for the ML model. We denote this ML model as the fatigue-stress ML model. After applying LASSO, the number of features is reduced to 19 from 42.

It is observed that the GPR model with the quadratic kernel, which was the best model for YS and UTS, is severely overfitted for the given set of features. The best model for fatigue is the GPR model with Matern kernel with R^2 of 0.96/0.96 and rmse of 0.32/0.32. Figure 2(d) represents the true versus predicted values for the GPR ML model for fatigue using stress as a feature. The ML model predicts the fatigue life for unknown data accurately.

To analyze the feature dependency of the ML model, Pearson correlation was calculated and is presented in Fig. 4(a). The figure shows that elements such as Mo, Nb, Fe, and Mn positively correlate with fatigue life, while elements such as C, Ni, and Co show a negative correlation with the number of cycles. Carbon is responsible for forming hard precipitate carbide phases in the microstructure. Although beneficial up to a certain extent for the creep properties, this precipitation is highly detrimental for the fatigue properties. The formation of rigid grain boundaries due to carbides often can serve as the initiation point of a crack in superalloys [141]. The negative correlation of nickel and cobalt is an obvious conclusion since the addition of larger amounts of γ' forming elements, fatigue, and creep enhancers reduce these elements. This trend is being captured as a negative correlation. In addition, the annealing conditions show a negative correlation with the fatigue life, indicating that severe annealing conditions can have an adverse effect on fatigue life due to prolonged heating.

The second ML model developed for fatigue life is based on the strain range the materials are subjected to in testing conditions (denoted as the fatigue-strain ML model). LASSO is applied on the feature set, which yields 19 important features for predicting fatigue life. The GPR models are trained using the four kernels. It is observed that the Matern kernel performs better than the quadratic, dot-product, and RBF kernels. Hence, the GRP model with the Matern kernel is employed for developing the ML model. The best result obtained for the GPR model is R^2 of 0.94/0.94 and rmse of 0.22/0.22. The GPR model with Matern kernel outperforms the quadratic kernel in fatigue models. Figure 2(e) represents the true versus predicted trends for the fatigue model with strain range. With its higher accuracy, this ML model is best suited for predicting fatigue life. The correlation analysis for the fatigue model is presented in Fig. 4(b). From Fig. 4(b), it is concluded that solid solution strengthening elements lead to an increase in the fatigue life, whereas elements such as carbon, phosphorus, and silicon lead to a decrease in fatigue life. The negative correlation of Re composition on fatigue
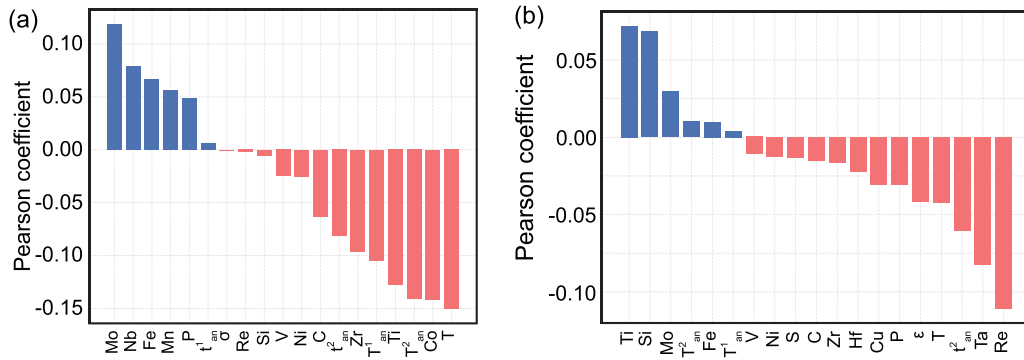
FIG. 4. Feature importance for fatigue life predicted through (a) stress range(MPa), (b) strain range (%).

life is an apparent departure from the experiments [142]. It is widely recognized that Re is responsible for the enhancement of fatigue and creep life of Ni-based superalloys. Re is generally added in constant and sparse quantities, making it difficult to determine the correlation with fatigue life accurately. The effect of Re on creep and fatigue properties has been analyzed further in the next section. Annealing temperatures show a small positive correlation and time shows a negative correlation. This implies that short annealing schedules at higher temperatures enhance fatigue properties. This is expected as fine grained alloys show superior fatigue performance due to delayed crack initiation. [143]. In addition, as expected, the temperature of fatigue, strain range, and stress range show a negative correlation, implying the reduction of fatigue life with an increase of any of these parameters. High temperature is known to enhance the cross slip in superalloys, leading to faster dislocation movement and defect formation [144].

Our paper aimed to build a framework such that a uniform set of features is deemed sufficient for calculating all the crucial mechanical properties. The primary features selected are mutually independent, as seen from Figs. S3– S7, with minimal cross correlations. The inclusion of these primary features is sufficient for accurate property prediction and it reduces the need for the calculation of other complex derived parameters for property prediction. Moreover, the ML models developed in this paper give a more accurate prediction without partitioning the data into different regimes, as usually seen in the case of the low-cycle and high-cycle fatigue or for the different mechanisms of creep rupture. GPR models with quadratic kernels provide very high accuracy for predicting YS and UTS, while Matern kernels are best suited for predicting creep and fatigue strength. The quadratic kernel is sufficient for accurate prediction since YS and UTS are properties with relatively more straightforward mechanisms. However, creep and fatigue strength are complex properties with several competing mechanisms and damage accumulation over time; therefore, it is difficult to model them using simpler kernel algorithms. Severe overfitting of the quadratic kernel-based models is a direct result of the same. On the other hand, GPR, which fits the data to an advanced kernel, is highly suited for predicting complex properties such as creep and fatigue strength. To compare with other ML algorithms, we also trained the models using SVR and XG-

Boost, presented in Supplemental Material Table 6. The ML models trained using other algorithms perform poorly when compared to the GPR models. The relatively low rmse values for all the GPR-based models in this paper demonstrate the effectiveness of the GPR for modeling the mechanical properties.

IV. DISCUSSION

To test the applicability of ML models developed in this paper, we performed validation tests by collecting new data to test the ML models [122,145–154]. The validation of the ML models was performed to check whether the ML models are able to predict properties of the unknown data set. We collected experimental data for all the mechanical properties, including YS, UTS, creep, and fatigue strength, and the corresponding composition, annealing, and testing parameters. In total, we collected 78 new data. The data was collected from literature and the source (DOI) of the data is present in Supplemental Material Table 1. The elemental features were generated for the new data set, and the data was then standardized using standard scalar with already fitted parameters. The data was then subjected to the same approach employed for the test data set. Each ML model developed has a different set of features for the prediction of the target property. We selected the features required from the new data to predict each mechanical property using our ML models. The results of the validation test are plotted in Figs. S8– S11. The validation results reveal that the ML models predict the mechanical properties of unknown data with high accuracy. All data lies within the range of ±0.5 from the black line, indicating highly precise predictions. Moreover, it can be observed that the ML models built in this paper can be utilized directly without any additional operations for predicting the properties of unique superalloys.

The ML models developed in this paper using GPR involve highly complex algorithms for training. This renders the ML models essentially as black boxes which are difficult to interpret directly. To analyze our best ML models, we employ SHapley Additive exPlanations (SHAP) to reveal the effect of individual features on the ML model [155–157]. The details of SHAP implementation are presented in the Supplemental Material. We study the effects of critical elemental concentrations on the creep and fatigue properties of the superalloys.
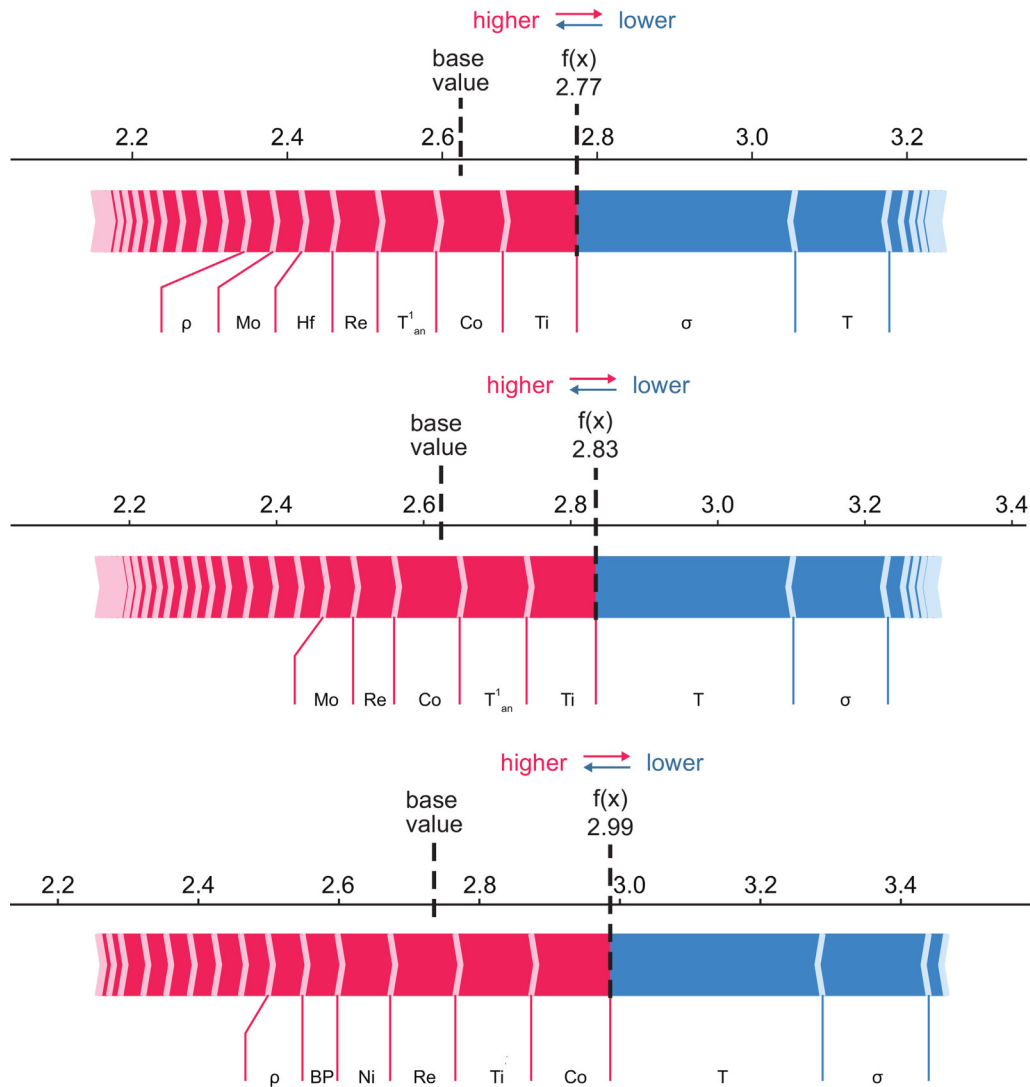
FIG. 5. SHAP force plot for some individual data set demonstrating the effects of rhenium addition on the creep rupture life of the material. The red arrows indicate that addition of a feature leads to increase of creep rupture life, while blue arrows represent that addition of the feature leads to decrease of rupture life.

One of the most important elements responsible for strengthening at high temperatures is rhenium. Rhenium is used for solid solution strengthening and enhances creep-resistance properties by arresting the growth of γ' phase particles by introducing more significant lattice misfits, which limit the movement of dislocations and diffusion of atoms [158–160]. In addition, the introduction of rhenium to superalloys can effectively increase fatigue resistance [46] of superalloys. From the ML models developed for creep and fatigue in this paper, it may initially seem that rhenium is not identified as an important parameter. However, through SHAP analysis of the ML model, we find that rhenium indeed plays a crucial role in increasing the creep resistance of superalloys. The SHAP force plot is shown in Fig. 5 to demonstrate the effect of rhenium. In Fig. 5, the base values represent the average value of the creep rupture life when no feature is revealed to the ML model. In this case, the ML model relies on the average values of all features in the data set. The red and blue arrows represent the effect of introducing individual features on the final output

value of creep rupture life. The red arrow represents that the addition of a feature leads to an increase in the rupture life over the base value, while the blue arrow represents that the addition of a feature value leads to a decrease in rupture life. The length of the arrows represents the magnitude or relative importance of an individual feature. From Fig. 5, it is observed that rhenium addition leads to a significant increase in the creep rupture life of superalloys. The contribution of rhenium for increasing the rupture life is similar in magnitude in most cases. The findings are similar to experimental study, where rhenium containing alloy shows the best creep properties because of solid solution strengthening in the γ phase and low diffusion coefficients at high temperatures, leading to effective resistance to dislocation motion in the γ [161]. From the force plot, it is also inferred that elements like titanium, cobalt, and molybdenum also contribute significantly in increasing the creep rupture life of a material. The temperature of creep test (T) and stress are the two most important factors that reduce the rupture life of superalloys.
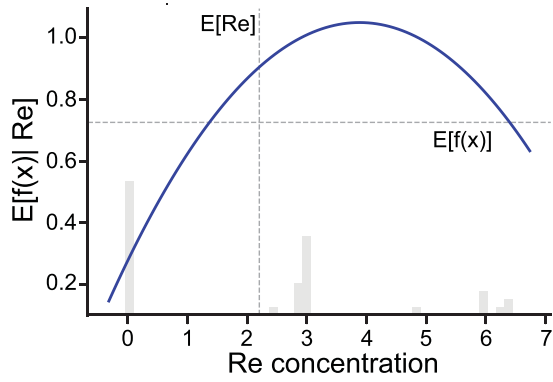
FIG. 6. SHAP dependence plot for rhenium addition on creep rupture life of the superalloys.

To further analyze the effect of elemental composition on creep and fatigue life of superalloys, we plot the dependence plot for elemental concentrations using SHAP. Figure 6 shows the dependence plot for rhenium addition on creep rupture life. The vertical line (E[Re]) represents the average composition of around 2% of rhenium and the horizontal line represents the expected value of the model. From Fig. 6, it is inferred that rhenium composition above 1.35% is highly beneficial for the creep properties of superalloys. According to the ML model developed, the best effect is observed for rhenium composition of 4%. The advantage of creep properties diminishes on further addition of rhenium. After the composition of 6.4%, the addition of rhenium becomes harmful for the superalloys. The results of the ML model are consistent with experimental results, where it is reported that the addition of large amounts of rhenium leads to precipitation of harmful TCP phases, which significantly decrease the creep resistance of superalloys [162,163]. Similarly, SHAP-dependence plot analysis for creep strengthening elements such as C, Cr, Co, Nb, Ta, Ti, W is presented in the Supplemental Material in Figs. S12– S18. The optimum range of compositions for the elements for increasing the creep rupture is predicted through the ML model. This range is presented in Table II. The formation of carbide phases limits the range of carbon addition. The ML model predicts that the elements Co, Cr, Ta, Ti, and W are beneficial in a wide composition range for creep rupture strength. A similar analysis for fatigue is presented in the Supplemental Material. The dependence plots for elemental concentrations for fatigue life are plotted in Figs. S-19– S-23.

TABLE III. Ideal range of composition (in %) for fatigue life.

Element	Lower limit	Upper limit
C	0	0.06
Co	0	7.6
Mo	0	2.75
Nb	0.15	4.4
Ti	2	

Using the best ML models for fatigue, we predicted the best range for different elements. The range of the ideal compositions are presented in Table III. It is seen that the addition of titanium and molybdenum has a significant impact on the fatigue life of superalloys. Similarly, adding cobalt in fewer quantities is beneficial for fatigue properties.

After accessing the feature importance for all the properties, it is essential to develop a framework encompassing a set of unified ML models for the mechanical properties that reflect the impact of all the important features. Developing such models is vital to capture all the intricate feature-property relationships of Ni-based superalloys. We analyzed all the GPR-based ML model features for all mechanical properties. The chosen features for individual property prediction are present in Figs. 3 and 4. It can be seen that the feature space varies widely for different properties. Therefore, we aim to identify standard features for developing the unifying ML models. While selecting features, it has to be ascertained that the features highly correlated to any mechanical property are not excluded. We first include all the features present in at least three of the five ML models developed, leading to the selection of 15 features. We observe that the compositions of some selected elements do not possess a significant correlation to any of the properties. We, therefore, drop these compositions and instead include all the annealing parameters and highly correlated compositions from each property. The list consists of 15 features using ML models for the mechanical properties which we developed. The results of the unified ML models are presented in Table IV. It can be observed that several ML models are developed for a wide range of mechanical properties through target selection of the highly correlated features. The unified ML models developed in this paper are developed using Python libraries and are exported using the Joblib library, making them highly transferable and directly employable for the prediction of mechanical properties without any additional requirements. To the best of

TABLE II. Ideal range of composition (in %) for creep rupture life.

Element	Lower limit	Upper limit
C	0	1
Co	0	12
Cr	0	14
Nb	0	0.3
Re	1.35	6.4
Ta	1	
Ti	0	1.2
W	0	7

TABLE IV. Results for the unifying ML models utilizing common set of features for prediction.

Property	GPR models	
	R^2	rmse
YS	0.96/0.96	0.11/0.11
UTS	0.98/0.97	0.07/0.08
Creep	0.99/0.97	0.15/0.28
Fatigue stress	0.96/0.95	0.74/0.75
Fatigue strain	0.95/0.94	0.51/0.51

the authors' knowledge, no such parallel framework exists in literature which predicts all the mechanical properties with high accuracy.

The results can be further improved if contributions from elements such as cerium and lanthanum, which are crucial for oxidation resistance of superalloys, are also added in the study. Since the focus of this paper is on mechanical properties only, we excluded the contribution from these elements. The presence of impurities such as sulfur, phosphorus, and nitrogen can also lead to local changes in the physical characteristics, which are not considered in this paper. Other parameters such as the microstructure and strain rate can also be explored in further research. In this paper, we explore ML-driven approaches to streamline and accelerate the process of discovery of unique superalloys. The approach will be useful for designing materials at reduced costs and can be extended to other classes of materials.

V. CONCLUSIONS

In this paper, we have developed a unified ML framework for predicting mechanical properties of Ni-based superalloys using the feature reduction technique LASSO and ML. Most basic features such as composition, heat treatment conditions, and mechanical testing conditions are employed in this study, and the most dominant features are selected using LASSO for ML model development. GPR-based models are used to predict YS, tensile strength, creep rupture life, and fatigue life (employing stress and strain as features). The ML models developed for the mechanical properties have unprecedented

accuracy. The ML models in this paper eliminate the need to partition the data for different regimes of creep and fatigue. The models show low errors when validated using unseen data from the literature. Further, SHAP analysis of the ML models developed reveals essential characteristics of the individual constituent elements. The ideal composition of elements is determined for creep and fatigue by analyzing the SHAP dependence plot. Finally, using feature engineering, we identify essential features for developing a unified ML framework for simultaneous prediction of all mechanical properties. The approach developed in this paper is highly transferable to other classes of materials/properties with minimal modifications.

The data required to reproduce these findings will be made available on GitHub.

[1] R. Reed and C. Rae, *Physical Metallurgy*, 5th ed. (Elsevier, UK, 2014), p. 2215.

[2] A. P. Mouritz, *Introduction to Aerospace Materials* (Woodhead Publishing, Cambridge, UK, 2012), p. 251.

[3] J. Cormier, X. Milhet, and J. Mendez, Non-isothermal creep at very high temperature of the nickel-based single crystal superalloy MC_2, Acta Mater. **55**, 6250 (2007).

[4] X. Zhou, T. Ma, Y. Li, L. Li, K. Wang, Y. Zhang, Y. Lai, and P. Zhang, Secondary γ' evolution and relationship to hot deformation behavior of a supersolvus-treated superalloy with high precipitate volume fraction, Mater. Sci. Eng. A. **761**, 138046 (2019).

[5] M. J. Donachie and S. J. Donachie, *Superalloys: A Technical Guide* (ASM international, Ohio, USA, 2002).

[6] P. Caron and T. Khan, Evolution of Ni-based superalloys for single crystal gas turbine blade applications, Aerosp. Sci. Technol. **3**, 513 (1999).

[7] R. Schafrik and R. Sprague, Gas turbine materials, Adv. Mater. Process **5**, 29 (2004).

[8] H. Long, S. Mao, Y. Liu, Z. Zhang, and X. Han, Microstructural and compositional design of Ni-based single crystalline superalloys—a review, J. Alloys Compd. **743**, 203 (2018).

[9] W. Xia, X. Zhao, L. Yue, and Z. Zhang, A review of composition evolution in Ni-based single crystal superalloys, J. Mater. Sci. Technol. **44**, 76 (2020).

[10] K. Kakehi, Effect of primary and secondary precipitates on creep strength of Ni-base superalloy single crystals, Mater. Sci. Eng. A **278**, 135 (2000).

[11] T. Murakumo, Y. Koizumi, K. Kobayashi, and H. Harada, Creep strength of Ni-base single-crystal superalloys on the γ/γ' tie-line, Superalloys **2004**, 155 (2004).

[12] E. Nembach and G. Neite, Precipitation hardening of superalloys by ordered γ'-particles, Prog. Mater. Sci. **29**, 177 (1985).

[13] A. Heckl, S. Neumeier, M. Göken, and R. Singer, The effect of Re and Ru on γ/γ' microstructure, γ-solid solution strengthening and creep strength in nickel-base superalloys, Mater. Sci. Eng. A **528**, 3435 (2011).

[14] B. Wang, J. Zhang, T. Huang, H. Su, Z. Li, L. Liu, and H. Fu, Influence of W, Re, Cr, and Mo on microstructural stability of the third generation Ni-based single crystal superalloys, J. Mater. Res. **31**, 3381 (2016).

[15] K. A. Christofidou, M. C. Hardy, H.-Y. Li, C. Argyrakis, H. Kitaguchi, N. G. Jones, P. M. Mignanelli, A. S. Wilson, O. M. Messé, E. J. Pickering *et al.*, On the effect of Nb on the microstructure and properties of next generation polycrystalline powder metallurgy Ni-based superalloys, Metall. Mater. Trans. A **49**, 3896 (2018).

[16] R. K. Barik and A. K. Singh, Accelerated discovery of the valley-polarized quantum anomalous Hall effect in MXenes, Chem. Mater. **33**, 6311 (2021).

[17] G. Pilania, C. Wang, X. Jiang, S. Rajasekaran, and R. Ramprasad, Accelerating materials property predictions using machine learning, Sci. Rep. **3**, 2810 (2013).

[18] R. Ramprasad, R. Batra, G. Pilania, A. Mannodi-Kanakkithodi, and C. Kim, Machine learning in materials informatics: Recent applications and prospects, Npj Comput. Mater. **3**, 54 (2017).

[19] Y. Liu, T. Zhao, W. Ju, and S. Shi, Materials discovery and design using machine learning, J. Materiomics **3**, 159 (2017).

[20] A. C. Rajan, A. Mishra, S. Satsangi, R. Vaish, H. Mizuseki, K.-R. Lee, and A. K. Singh, Machine-learning-assisted accurate band gap predictions of functionalized MXene, Chem. Mater. **30**, 4031 (2018).

[21] J. Lee, A. Seko, K. Shitara, K. Nakayama, and I. Tanaka, Prediction model of band gap for inorganic compounds by combination of density functional theory calculations and machine learning techniques, Phys. Rev. B **93**, 115104 (2016).

[22] R. Gurnani, D. Kamal, H. Tran, H. Sahu, K. Scharm, U. Ashraf, and R. Ramprasad, polyg2g: A novel machine learning algorithm applied to the generative design of polymer dielectrics, Chem. Mater. **33**, 7008 (2021).

[23] A. Mishra, S. Satsangi, A. C. Rajan, H. Mizuseki, K.-R. Lee, and A. K. Singh, Accelerated data-driven accurate positioning of the band edges of MXenes, J. Phys. Chem. Lett. **10**, 780 (2019).

[24] R. Juneja, G. Yumnam, S. Satsangi, and A. K. Singh, Coupling the high-throughput property map to machine learning for predicting lattice thermal conductivity, Chem. Mater. **31**, 5145 (2019).

[25] C. Kim, A. Chandrasekaran, A. Jha, and R. Ramprasad, Active-learning and materials design: the example of high glass transition temperature polymers, MRS Commun. **9**, 860 (2019).

[26] L. Chen, C. Kim, R. Batra, J. P. Lightstone, C. Wu, Z. Li, A. A. Deshmukh, Y. Wang, H. D. Tran, P. Vashishta *et al.*, Frequency-dependent dielectric constant prediction of polymers using machine learning, Npj Comput. Mater. **6**, 1 (2020).

[27] S. Swetlana, N. Khatavkar, and A. K. Singh, Development of Vickers hardness prediction models via microstructural analysis and machine learning, J. Mater. Sci. **55**, 15845 (2020).

[28] N. Khatavkar, S. Swetlana, and A. K. Singh, Accelerated prediction of Vickers hardness of Co-and Ni-based superalloys from microstructure and composition using advanced image processing techniques and machine learning, Acta Mater. **196**, 295 (2020).

[29] W. Huang, P. Martin, and H. L. Zhuang, Machine-learning phase prediction of high-entropy alloys, Acta Mater. **169**, 225 (2019).

[30] C. Wen, Y. Zhang, C. Wang, D. Xue, Y. Bai, S. Antonov, L. Dai, T. Lookman, and Y. Su, Machine learning assisted design of high entropy alloys with desired property, Acta Mater. **170**, 109 (2019).

[31] K. Kaufmann and K. S. Vecchio, Searching for high entropy alloys: A machine learning approach, Acta Mater. **198**, 178 (2020).

[32] B. Conduit, N. G. Jones, H. J. Stone, and G. J. Conduit, Design of a nickel-base superalloy using a neural network, Mater. Des. **131**, 358 (2017).

[33] P. L. Taylor and G. Conduit, Machine learning predictions of superalloy microstructure, Comput. Mater. Sci. **201**, 110916 (2022).

[34] Y. Zhang and X. Xu, Lattice misfit predictions via the Gaussian process regression for Ni-based single crystal superalloys, Met. Mater. Int. **27**, 235 (2021).

[35] H. Hong, J. Kang, B. G. Choi, I. Kim, Y. Yoo, and C. Jo, A comparative study on thermomechanical and low cycle fatigue failures of a single crystal nickel-based superalloy, Int. J. Fatigue **33**, 1592 (2011).

[36] P. R. Barrett, R. Ahmed, M. Menon, and T. Hassan, Isothermal low-cycle fatigue and fatigue-creep of Haynes 230, Int. J. Solids Struct. **88-89**, 146 (2016).

[37] B. Du, J. Yang, C. Cui, and X. Sun, Effects of grain size on the high-cycle fatigue behavior of IN792 superalloy, Mater. Des. **65**, 57 (2015).

[38] A. Sengupta, S. Putatunda, L. Bartosiewicz, J. Hangas, P. Nailos, M. Peputapeck, and F. Alberts, Tensile behavior of a new single-crystal nickel-based superalloy (CMSX-4) at room and elevated temperatures, J. Mater. Eng. Perform. **3**, 73 (1994).

[39] T. Khan and P. Caron, Effect of processing conditions and heat treatments on mechanical properties of single-crystal superalloy CMSX-2, Mater. Sci. Technol. **2**, 486 (1986).

[40] B. Wilson, E. Cutler, and G. Fuchs, Effect of solidification parameters on the microstructures and properties of CMSX-10, Mater. Sci. Eng. A **479**, 356 (2008).

[41] L. Liu, T. Huang, J. Zhang, and H. Fu, Microstructure and stress rupture properties of single crystal superalloy CMSX-2 under high thermal gradient directional solidification, Mater. Lett. **61**, 227 (2007).

[42] K. Harris and J. B. Wahl, Improved single crystal superalloys, CMSX-4 (SLS)[La+Y] and CMSX-486, Superalloys **2004**, 45 (2004).

[43] M. Acharya and G. Fuchs, The effect of long-term thermal exposures on the microstructure and properties of CMSX-10 single crystal Ni-base superalloys, Mater. Sci. Eng. A **381**, 143 (2004).

[44] K. Harris, G. Erickson, and R. Schwer, MAR-M247 derivations-CM247 LC DS alloy, CMSX single crystal alloys, properties and performance, Superalloys 221 (1984).

[45] J. Veys and R. Mevrel, Influence of protective coatings on the mechanical properties of CMSX-2 and Cotac 784, Mater. Sci. Eng. **88**, 253 (1987).

[46] G. Erickson, The development and application of CMSX-10, Superalloys 35 (1996).

[47] K. Fullagar, R. Broomfield, M. Hulands, K. Harris, G. Erickson, and S. Sikkenga, Aero engine test experience with CMSX-4® alloy single-crystal turbine blades, J. Eng. Gas Turbines Power **118**, 380 (1996).

[48] J. B. Wahl and K. Harris, New single crystal superalloys, CMSX®-8 and CMSX®-7, in *Turbo Expo: Power for Land, Sea, and Air* (American Society of Mechanical Engineers, Düsseldorf, Germany, 2014), Vol. 45752, p. V006T22A002.

[49] P. Xia, J. Yu, X. Sun, H. Guan, and Z. Hu, Influence of thermal exposure on γ' precipitation and tensile properties of DZ951 alloy, Mater. Charact. **58**, 645 (2007).

[50] C. Körner, M. Ramsperger, C. Meid, D. Bürger, P. Wollgramm, M. Bartsch, and G. Eggeler, Microstructure and mechanical properties of CMSX-4 single crystals prepared

by additive manufacturing, Metall. Mater. Trans. A **49**, 3781 (2018).

[51] V. Sabelkin, G. Joshi, S. Mall, W. Porter, and R. John, Monotonic tension and creep behavior of single crystal CMSX-486 under combustion environment, Mater. Sci. Eng. A **569**, 106 (2013).

[52] J. Lapin, T. Pelachová, and O. Bajana, The effect of microstructure on mechanical properties of single crystal CMSX-4 superalloy, in *Proceedings of the 22nd International Conference on Metallurgy and Materials, Metal* (Tanger, Brno, Czech Republic, EU, 2013), p. 1277.

[53] T. Coppola, S. Riscifuli, O. Tassa, and G. Pasquero, Thermomechanical fatigue behavior of bare and coated CMSX-4, J. Eng. Gas Turbines Power **132**, 012101 (2010).

[54] A. Sengupta and S. K. Putatunda, Dynamic strain aging in a new single crystal nickel-based superalloy (CMSX-4), J. Test. Eval. **23**, 87 (1995).

[55] A. Sato, J. J. Moverare, M. Hasselqvist, and R. C. Reed, On the mechanical behavior of a new single-crystal superalloy for industrial gas turbine applications, Metall. Mater. Trans. A **43**, 2302 (2012).

[56] J. Lapin, T. Pelachova, and M. Gebura, The effect of creep exposure on microstructure stability and tensile properties of single crystal nickel based superalloy CMSX-4, Kovove Mater. **50**, 379 (2012).

[57] R. Reed, N. Matan, D. Cox, M. Rist, and C. Rae, Creep of CMSX-4 superalloy single crystals: Effects of rafting at high temperature, Acta Mater. **47**, 3367 (1999).

[58] A. Sato, H. Harada, A.-C. Yeh, K. Kawagishi, T. Kobayashi, Y. Koizumi, T. Yokokawa, and J. Zhang, A 5th generation SC superalloy with balanced high temperature properties and processability, Superalloys 131 (2008).

[59] A. Basak and S. Das, Effect of heat treatment on the microstructures of CMSX-4® processed through scanning laser epitaxy (SLE), in *2017 International Solid Freeform Fabrication Symposium* (University of Texas at Austin, Austin, Texas, USA, 2017).

[60] J. B. Wahl and K. Harris, Improved 3rd generation single crystal superalloy CMSX-4® plus (SLS)-a study of evolutionary alloy development (Cannon-Muskegon, Muskegon, MI, 1984).

[61] M. D. Fitzpatrick, W. D. Brentnall, A. Meier, G. L. Erickson, and G. DeBoer, Design of a high efficiency industrial turbine blade utilizing third generation single crystal alloy CMSX®-10, in *Turbo Expo: Power for Land, Sea, and Air* (American Society of Mechanical Engineers, Orlando, Florida, USA, 1997), Vol. 78712, p. V004T12A022.

[62] K. Kobayashi, K. Yamaguchi, M. Hayakawa, and M. Kimura, High-temperature fatigue properties of austenitic superalloys 718, A286 and 304L, Int. J. Fatigue **30**, 1978 (2008).

[63] M. Lamm and R. Singer, The effect of casting conditions on the high-cycle fatigue properties of the single-crystal nickel-base superalloy PWA 1483, Metall. Mater. Trans. A **38**, 1177 (2007).

[64] J. Tian, J. Villegas, W. Yuan, D. Fielden, L. Shaw, P. Liaw, and D. Klarstrom, A study of the effect of nanostructured surface layers on the fatigue behaviors of a C-2000 superalloy, Mater. Sci. Eng. A **468-470**, 164 (2007).

[65] K. Rahmani and S. Nategh, Influence of aluminide diffusion coating on low cycle fatigue properties of René 80, Mater. Sci. Eng. A **486**, 686 (2008).

[66] S. Lee, Y. Lu, P. Liaw, L. Chen, S. Thompson, J. Blust, P. Browning, A. Bhattacharya, J. Aurrecoechea, and D. Klarstrom, Tensile-hold low-cycle-fatigue properties of solid-solution-strengthened superalloys at elevated temperatures, Mater. Sci. Eng. A **504**, 64 (2009).

[67] Z. Shi, X. Wang, S. Liu, and J. Li, Low cycle fatigue properties and microstructure evolution at 760°C of a single crystal superalloy, Prog. Nat. Sci.: Mater. Int. **25**, 78 (2015).

[68] T. Billot, P. Villechaise, M. Jouiad, and J. Mendez, Creep–fatigue behavior at high temperature of a UDIMET 720 nickel-base superalloy, Int. J. Fatigue **32**, 824 (2010).

[69] R. Kowalewski and H. Mughrabi, Influence of a plasma-sprayed NiCrAlY coating on the low-cycle fatigue behaviour of a directionally solidified nickel-base superalloy, Mater. Sci. Eng. A **247**, 295 (1998).

[70] Y. Ro, H. Zhou, Y. Koizumi, T. Yokokawa, T. Kobayashi, H. Harada, and I. Okada, Thermal-mechanical fatigue property of Ni-base single crystal superalloys TMS-82+ and TMS-75, Mater. Trans. **45**, 396 (2004).

[71] M. Aydinöz, F. Brenne, M. Schaper, C. Schaak, W. Tillmann, J. Nellesen, and T. Niendorf, On the microstructural and mechanical properties of post-treated additively manufactured Inconel 718 superalloy under quasi-static and cyclic loading, Mater. Sci. Eng. A **669**, 246 (2016).

[72] L. Chen, Z. Wang, G. Yao, and J. Tian, The influence of temperature on low cycle fatigue behavior of nickel base superalloy GH4049, Int. J. Fatigue **21**, 791 (1999).

[73] J. Yu, X. Sun, T. Jin, N. Zhao, H. Guan, and Z. Hu, High temperature creep and low cycle fatigue of a nickel-base superalloy, Mater. Sci. Eng. A **527**, 2379 (2010).

[74] P. Zhang, Q. Zhu, C. Hu, C.-j. Wang, G. Chen, and H.-y. Qin, Cyclic deformation behavior of a nickel-base superalloy under fatigue loading, Mater. Des. **69**, 12 (2015).

[75] H.-E. Huang and C.-H. Koo, Characteristics and mechanical properties of polycrystalline CM 247 LC superalloy casting, Mater. Trans. **45**, 562 (2004).

[76] J. Gayda and R. Miner, Fatigue crack initiation and propagation in several nickel-base superalloys at 650 C, Int. J. Fatigue **5**, 135 (1983).

[77] J. Miao, T. M. Pollock, and J. W. Jones, Crystallographic fatigue crack initiation in nickel-based superalloy René 88DT at elevated temperature, Acta Mater. **57**, 5964 (2009).

[78] A. Mostafaei, S. H. V. R. Neelapu, C. Kisailus, L. M. Nath, T. D. Jacobs, and M. Chmielus, Characterizing surface finish and fatigue behavior in binder-jet 3D-printed nickel-based superalloy 625, Addit. Manuf. **24**, 200 (2018).

[79] Y. Itoh, M. Saitoh, and Y. Ishiwata, Influence of high-temperature protective coatings on the mechanical properties of nickel-based superalloys, J. Mater. Sci. **34**, 3957 (1999).

[80] Y. Jinxia, Q. Zheng, S. Xiaofeng, G. Hengrong, and H. Zhuangqi, Thermal fatigue behavior of K465 superalloy, Rare Met. **25**, 202 (2006).

[81] M. Ott and H. Mughrabi, Dependence of the high-temperature low-cycle fatigue behaviour of the monocrystalline nickel-base superalloys CMSX-4 and CMSX-6 on the γ/γ' morphology, Mater. Sci. Eng. A **272**, 24 (1999).

[82] J. Gayda, T. Gabb, and R. Miner, Fatigue crack propagation of nickel-base superalloys at 650 °C, in *Symp. on Low-Cycle Fatigue Directions for the Future*, NAS 1.15: 87150 (ASTM International, New York, USA, 1985).

[83] J. Li and R. Wahi, Investigation of γ/γ' lattice mismatch in the polycrystalline nickel-base superalloy IN738LC : Influence of heat treatment and creep deformation, Acta Metall. Mater. **43**, 507 (1995).

[84] C. Cui, Y. Gu, Y. Yuan, T. Osada, and H. Harada, Enhanced mechanical properties in a new Ni–Co base superalloy by controlling microstructures, Mater. Sci. Eng. A **528**, 5465 (2011).

[85] P. Li, S.-S. Li, and Y.-S. Han, Influence of solution heat treatment on microstructure and stress rupture properties of a Ni3Al base single crystal superalloy IC6SX, Intermetallics **19**, 182 (2011).

[86] L.-R. Liu, T. Jin, N.-R. Zhao, Z. Wang, X. Sun, H. Guan, and Z. Hu, Effect of carbon addition on the creep properties in a Ni-based single crystal superalloy, Mater. Sci. Eng. A **385**, 105 (2004).

[87] X. Qin, J. Guo, C. Yuan, J. Hou, L. Zhou, and H. Ye, Long-term thermal exposure responses of the microstructure and properties of a cast Ni-base superalloy, Mater. Sci. Eng. A **543**, 121 (2012).

[88] C. Tian, G. Han, C. Cui, and X. Sun, Effects of Co content on tensile properties and deformation behaviors of Ni-based disk superalloys at different temperatures, Mater. Des. **88**, 123 (2015).

[89] D. Kaoumi and K. Hrutkay, Tensile deformation behavior and microstructure evolution of Ni-based superalloy 617, J. Nucl. Mater. **454**, 265 (2014).

[90] X. Xiong, D. Quan, P. Dai, Z. Wang, Q. Zhang, and Z. Yue, Tensile behavior of nickel-base single-crystal superalloy DD6, Mater. Sci. Eng. A **636**, 608 (2015).

[91] C. Boehlert and S. Longanbach, A comparison of the microstructure and creep behavior of cold rolled HAYNES ® 230 alloy and HAYNES ® 282 alloy, Mater. Sci. Eng. A **528**, 4888 (2011).

[92] K. Hrutkay and D. Kaoumi, Tensile deformation behavior of a nickel based superalloy at different temperatures, Mater. Sci. Eng. A **599**, 196 (2014).

[93] G. Chen, Y. Zhang, D. Xu, Y. Lin, and X. Chen, Low cycle fatigue and creep-fatigue interaction behavior of nickel-base superalloy GH4169 at elevated temperature of 650 C, Mater. Sci. Eng. A **655**, 175 (2016).

[94] I. Kim, B. Choi, H. Hong, J. Do, and C. Jo, Influence of thermal exposure on the microstructural evolution and mechanical properties of a wrought Ni-base superalloy, Mater. Sci. Eng. A **593**, 55 (2014).

[95] D.-X. Wen, Y. Lin, J. Chen, X.-M. Chen, J.-L. Zhang, Y.-J. Liang, and L.-T. Li, Work-hardening behaviors of typical solution-treated and aged Ni-based superalloys during hot deformation, J. Alloys Compd. **618**, 372 (2015).

[96] J. Wang, W.-G. Guo, Y. Su, P. Zhou, and K. Yuan, Anomalous behaviors of a single-crystal Nickel-base superalloy over a wide range of temperatures and strain rates, Mech. Mater. **94**, 79 (2016).

[97] T. Wang, C. Wang, W. Sun, X. Qin, J. Guo, and L. Zhou, Microstructure evolution and mechanical properties of GH984G

[98] J. Shingledecker, N. Evans, and G. Pharr, Influences of composition and grain size on creep–rupture behavior of Inconel® alloy 740, Mater. Sci. Eng. A **578**, 277 (2013).

[99] F. Yang, E. Liu, Z. Zhi, J. Tong, and L. Ning, Influence of Ti content on microstructure, mechanical properties and castability of directionally solidified superalloy DZ125L, Mater. Des. **61**, 41 (2014).

[100] X. Wang, J. Liu, T. Jin, and X. Sun, Tensile behaviors and deformation mechanisms of a nickel-base single crystal superalloy at different temperatures, Mater. Sci. Eng. A **598**, 154 (2014).

[101] Y. Yuan, Y. Gu, C. Cui, T. Osada, T. Tetsui, T. Yokokawa, and H. Harada, Creep mechanisms of U720Li disc superalloy at intermediate temperature, Mater. Sci. Eng. A **528**, 5106 (2011).

[102] J. Zhang, T. Murakumo, Y. Koizumi, and H. Harada, The influence of interfacial dislocation arrangements in a fourth generation single crystal TMS-138 superalloy on creep properties, J. Mater. Sci. **38**, 4883 (2003).

[103] H. Bor, C. Chao, and C. Ma, The influence of magnesium on carbide characteristics and creep behavior of the Mar-M247 superalloy, Scr. Mater. **38**, 329 (1997).

[104] See Supplemental Material at http://link.aps.org/supplemental/10.1103/PhysRevMaterials.6.123603 for details regarding the data, ML models, and supplemental figures.

[105] R. Tibshirani, Regression shrinkage and selection via the lasso, J. R. Stat. Soc., B: Stat. Methodol **58**, 267 (1996).

[106] Y. Liu, B. Guo, X. Zou, Y. Li, and S. Shi, Machine learning assisted materials design and discovery for rechargeable batteries, Energy Storage Mater. **31**, 434 (2020).

[107] Y. Liu, J.-M. Wu, M. Avdeev, and S.-Q. Shi, Multi-layer feature selection incorporating weighted score-based expert knowledge toward modeling materials with targeted properties, Adv. Theory Simul. **3**, 1900215 (2020).

[108] K. P. Murphy, *Machine Learning: A Probabilistic Perspective* (MIT Press, Cambridge, UK, 2012).

[109] J. Quinonero-Candela and C. E. Rasmussen, A unifying view of sparse approximate Gaussian process regression, J. Mach. Learn. Res. **6**, 1939 (2005).

[110] J. Benesty, J. Chen, Y. Huang, and I. Cohen, *Noise Reduction in Speech Processing* (Springer, Berlin, Heidelberg, 2009).

[111] F. Pedregosa, G. Varoquaux, A. Gramfort, V. Michel, B. Thirion, O. Grisel, M. Blondel, P. Prettenhofer, R. Weiss, V. Dubourg *et al.*, Scikit-learn: Machine learning in Python, J. Mach. Learn. Res. **12**, 2825 (2011).

[112] X. Zhou, F. Zhou, and M. Naseri, An insight into the estimation of frost thermal conductivity on parallel surface channels using kernel based GPR strategy, Sci. Rep. **11**, 7203 (2021).

[113] G. A. Rao, M. Kumar, M. Srinivas, and D. Sarma, Effect of standard heat treatment on the microstructure and mechanical properties of hot isostatically pressed superalloy Inconel 718, Mater. Sci. Eng. A **355**, 114 (2003).

[114] R. E. Smallman, *Modern Physical Metallurgy* (Elsevier, UK, 2016).

[115] A. K. Roy and A. Venkatesh, Evaluation of yield strength anomaly of alloy 718 at 700-800 °C, J. Alloys Compd. **496**, 393 (2010).

[116] P. Geng, W. Li, X. Zhang, Y. Deng, H. Kou, J. Ma, J. Shao, L. Chen, and X. Wu, A theoretical model for yield strength anomaly of Ni-base superalloys at elevated temperature, J. Alloys Compd. **706**, 340 (2017).

[117] D. J. Crudden, B. Raeisinia, N. Warnken, and R. C. Reed, Analysis of the chemistry of Ni-base turbine disk superalloys using an alloys-by-design modeling approach, Metall. Mater. Trans. A **44**, 2418 (2013).

[118] D. Collins and H. Stone, A modelling approach to yield strength optimisation in a nickel-base superalloy, Int. J. Plast. **54**, 96 (2014).

[119] X. Zhang, W. Li, J. Ma, P. Geng, J. Shao, and X. Wu, A novel temperature dependent yield strength model for metals considering precipitation strengthening and strain rate, Comput. Mater. Sci. **129**, 147 (2017).

[120] Y.-K. Kim, D. Kim, H.-K. Kim, E.-Y. Yoon, Y. Lee, C.-S. Oh, and B.-J. Lee, A numerical model to predict mechanical properties of Ni-base disk superalloys, Int. J. Plast. **110**, 123 (2018).

[121] Y. Yoo, I. Kim, D. Kim, C. Jo, H. Kim, and C. Jones, The application of neural network to the development of single crystal superalloys, Superalloys 942 (2004).

[122] C.-N. Wei, H.-Y. Bor, and L. Chang, The effects of carbon content on the microstructure and elevated temperature tensile strength of a nickel-base superalloy, Mater. Sci. Eng. A **527**, 3741 (2010).

[123] E. Balikci, A. Raman, and R. Mirshams, Tensile strengthening in the nickel-base superalloy IN738LC, J. Mater. Eng. Perform. **9**, 324 (2000).

[124] G. Bai, J. Li, R. Hu, Z. Tang, X. Xue, and H. Fu, Effect of temperature on tensile behavior of Ni–Cr–W based superalloy, Mater. Sci. Eng. A **528**, 1974 (2011).

[125] D. Bürger, A. Parsa, M. Ramsperger, C. Körner, and G. Eggeler, Creep properties of single crystal Ni-base superalloys (SX): A comparison between conventionally cast and additive manufactured CMSX-4 materials, Mater. Sci. Eng. A **762**, 138098 (2019).

[126] B. Du, Z. Hu, L. Sheng, C. Cui, J. Yang, Y. Zheng, and X. Sun, Tensile, creep behavior and microstructure evolution of an as-cast Ni-based K417G polycrystalline superalloy, J. Mater. Sci. Technol. **34**, 1805 (2018).

[127] W. Harrison, M. Whittaker, and S. Williams, Recent advances in creep modelling of the nickel base superalloy, alloy 720Li, Materials **6**, 1118 (2013).

[128] A. Ma, D. Dye, and R. Reed, A model for the creep deformation behaviour of single-crystal superalloy CMSX-4, Acta Mater. **56**, 1657 (2008).

[129] A. Staroselsky and B. N. Cassenti, Creep, plasticity, and fatigue of single crystal superalloy, Int. J. Solids Struct. **48**, 2060 (2011).

[130] D. MacLachlan and D. Knowles, Creep-behavior modeling of the single-crystal superalloy CMSX-4, Metall. Mater. Trans. A **31**, 1401 (2000).

[131] W. Xia, X. Zhao, L. Yue, and Z. Zhang, Microstructural evolution and creep mechanisms in Ni-based single crystal superalloys: A review, J. Alloys Compd. **819**, 152954 (2020).

[132] Z. Zhu, H. Basoalto, N. Warnken, and R. Reed, A model for the creep deformation behaviour of nickel-based single crystal superalloys, Acta Mater. **60**, 4888 (2012).

[133] R. MacKay, T. Gabb, and M. Nathal, Microstructure-sensitive creep models for nickel-base superalloy single crystals, Mater. Sci. Eng. A **582**, 397 (2013).

[134] P. Wollgramm, H. Buck, K. Neuking, A. Parsa, S. Schuwalow, J. Rogal, R. Drautz, and G. Eggeler, On the role of Re in the stress and temperature dependence of creep of Ni-base single crystal superalloys, Mater. Sci. Eng. A **628**, 382 (2015).

[135] Z. Peng, G. Tian, J. Jiang, M. Li, Y. Chen, J. Zou, and F. P. Dunne, Mechanistic behaviour and modelling of creep in powder metallurgy FGH96 nickel superalloy, Mater. Sci. Eng. A **676**, 441 (2016).

[136] Y. Liu, J. Wu, Z. Wang, X.-G. Lu, M. Avdeev, S. Shi, C. Wang, and T. Yu, Predicting creep rupture life of Ni-based single crystal superalloys using divide-and-conquer approach based machine learning, Acta Mater. **195**, 454 (2020).

[137] D. Shin, Y. Yamamoto, M. P. Brady, S. Lee, and J. A. Haynes, Modern data analytics approach to predict creep of high-temperature alloys, Acta Mater. **168**, 321 (2019).

[138] Y. Yoo, C. Jo, and C. Jones, Compositional prediction of creep rupture life of single crystal Ni-base superalloy by Bayesian neural network, Mater. Sci. Eng. A **336**, 22 (2002).

[139] Y. Xu, Q. Jin, X. Xiao, X. Cao, G. Jia, Y. Zhu, and H. Yin, Strengthening mechanisms of carbon in modified nickel-based superalloy Nimonic 80A, Mater. Sci. Eng. A. **528**, 4600 (2011).

[140] L. Wang, D. Wang, T. Liu, X. Li, W. Jiang, G. Zhang, and L. Lou, Effect of minor carbon additions on the high-temperature creep behavior of a single-crystal nickel-based superalloy, Mater. Charact. **104**, 81 (2015).

[141] R. Jiang, D. Bull, A. Evangelou, A. Harte, F. Pierron, I. Sinclair, M. Preuss, X. Hu, and P. Reed, Strain accumulation and fatigue crack initiation at pores and carbides in a SX superalloy at room temperature, Int. J. Fatigue **114**, 22 (2018).

[142] M. Huang and J. Zhu, An overview of rhenium effect in single-crystal superalloys, Rare Metals **35**, 127 (2016).

[143] R. Jiang, N. Karpasitis, N. Gao, and P. Reed, Effects of microstructures on fatigue crack initiation and short crack propagation at room temperature in an advanced disc superalloy, Mater. Sci. Eng. A. **641**, 148 (2015).

[144] A. Pineau and S. D. Antolovich, High temperature fatigue of nickel-base superalloys–a review with special emphasis on deformation modes and oxidation, Eng. Fail. Anal. **16**, 2668 (2009).

[145] A. Cervellon, J. Cormier, F. Mauget, Z. Hervier, and Y. Nadot, Very high cycle fatigue of Ni-based single-crystal superalloys at high temperature, Metall. Mater. Trans. A **49**, 3938 (2018).

[146] T. Murakumo, T. Kobayashi, Y. Koizumi, and H. Harada, Creep behaviour of Ni-base single-crystal superalloys with various γ' volume fraction, Acta Mater. **52**, 3737 (2004).

[147] A.-C. Yeh, A. Sato, T. Kobayashi, and H. Harada, On the creep and phase stability of advanced Ni-base single crystal superalloys, Mater. Sci. Eng. A **490**, 445 (2008).

[148] C. Cui, Y. Gu, D. Ping, and H. Harada, Microstructural evolution and mechanical properties of a Ni-based superalloy, TMW-4, Metall. Mater. Trans. A **40**, 282 (2009).

[149] L. Gong, B. Chen, L. Zhang, Y. Ma, and K. Liu, Effect of cooling rate on microstructure, microsegregation and mechanical properties of cast Ni-based superalloy K417G, J. Mater. Sci. Technol. **34**, 811 (2018).

[150] Z. Lian, J. Yu, X. Sun, H. Guan, and Z. Hu, Temperature dependence of tensile behavior of Ni-based superalloy M951, Mater. Sci. Eng. A **489**, 227 (2008).

[151] Y. Gu, H. Harada, C. Cui, D. Ping, A. Sato, and J. Fujioka, New Ni-Co base disk superalloys with higher strength and creep resistance, Scr. Mater. **55**, 815 (2006).

[152] L. Tan, Y. Li, W. Deng, Y. Liu, F. Liu, Y. Nie, and L. Jiang, Tensile properties of three newly developed Ni-base powder metallurgy superalloys, J. Alloys Compd. **804**, 322 (2019).

[153] P. Zhang, Y. Yuan, J. Li, Y. Xu, X. Song, and G. Yang, Tensile deformation mechanisms in a new directionally solidified Ni-base superalloy containing coarse γ' precipitates at 650 °C, Mater. Sci. Eng. A **702**, 343 (2017).

[154] S. Jha, M. Caton, and J. Larsen, Mean vs. life-limiting fatigue behavior of a nickel-based superalloy, Superalloys 565 (2008).

[155] S. M. Lundberg and S.-I. Lee, A unified approach to interpreting model predictions, Adv. Neural. Inf. Process. Syst. **30**, 1 (2017).

[156] S. M. Lundberg, B. Nair, M. S. Vavilala, M. Horibe, M. J. Eisses, T. Adams, D. E. Liston, D. K.-W. Low, S.-F. Newman, J. Kim *et al.*, Explainable machine-learning predictions for the prevention of hypoxaemia during surgery, Nat. Biomed. Eng. **2**, 749 (2018).

[157] S. M. Lundberg, G. Erion, H. Chen, A. DeGrave, J. M. Prutkin, B. Nair, R. Katz, J. Himmelfarb, N. Bansal, and S.-I. Lee, From local explanations to global understanding with explainable AI for trees, Nat. Mach. Intell. **2**, 56 (2020).

[158] R. C. Reed, *The Superalloys: Fundamentals and Applications* (Cambridge University Press, Cambridge, UK, 2008).

[159] K. Harris, G. Erickson, S. Sikkenga, W. Brentnall, J. Aurrecoechea, and K. Kubarych, Development of two rhenium-containing superalloys for single-crystal blade and directionally solidified vane applications in advanced turbine engines, J. Mater. Eng. Perform. **2**, 481 (1993).

[160] T. M. Pollock, The growth and elevated temperature stability of high refractory nickel-base single crystals, Mater. Sci. Eng. B **32**, 255 (1995).

[161] S. Giese, A. Bezold, M. Pröbstle, A. Heckl, S. Neumeier, and M. Göken, The importance of diffusivity and partitioning behavior of solid solution strengthening elements for the high temperature creep strength of Ni-base superalloys, Metall. Mater. Trans. A **51**, 6195 (2020).

[162] K. Cheng, C. Jo, D. Kim, T. Jin, and Z. Hu, Unexpected precipitation of a Re-rich phase in single crystal superalloy CMSX-4 during thermal exposure, J. Metall. **2012**, 308568 (2012).

[163] R. Jayaram and M. Miller, Influence of phase composition and microstructure on the high temperature creep properties of a model single crystal nickel-base superalloy: An atom probe/AEM study, Acta Metall. Mater. **43**, 1979 (1995).